Computers and Chemical Engineering 134 (2020) 106685

Contents lists available at ScienceDirect

Computers and Chemical Engineering

journal homepage: www.elsevier.com/locate/compchemeng

Comparison of intrusive and nonintrusive polynomial chaos expansion-based approaches for high dimensional parametric uncertainty quantification and propagation

Jeongeun Son, Yuncheng Du*

Department of Chemical and Biomolecular Engineering, Clarkson University, Potsdam, NY 13699, USA

ARTICLE INFO

Article history:
Received 26 September 2019
Revised 7 November 2019
Accepted 20 December 2019
Available online 24 December 2019

Keywords:
Generalized dimension reduction
Generalized polynomial chaos
Parametric uncertainty
Stochastic collocation
Penicillin production
Autocrine signalling of living cells

ABSTRACT

We present an uncertainty quantification (UQ) algorithm using the intrusive generalized polynomial chaos (gPC) expansion in combination with dimension reduction techniques and compare the UQ accuracy and computational efficiency of the intrusive gPC-based UQ algorithm to other sampling-based nonintrusive methods. The successful application of intrusive gPC-based UQ is associated with the stochastic Galerkin (SG) projection, which yields a family of models described by several coupled equations of gPC coefficients. Using these coefficients, the evolution of uncertainty in a dynamic system can be quickly determined when there is probabilistic uncertainty in the system. While elegant, when dealing with models that involve complex functions (e.g., nonpolynomial terms) and larger numbers of uncertainties, SG projection becomes computationally intractable and cannot be applied directly to solve gPC coefficients in real-time. To address this issue, the generalized dimension reduction method (gDRM) is used to convert a high-dimensional integral involved in the SG projection into several lower-dimensional integrals that can be easily solved. To show the accuracy of UQ, the algorithm in this work is compared to sampling-based approaches such as the nonintrusive stochastic collocation (SC) and Monte Carlo (MC) simulations using three cases: a nonlinear algebraic benchmark, a penicillin manufacturing process, and autocrine signalling networks of living cells.

1. Introduction

Mathematical modelling and simulations are important tools to describe dynamic behaviour of complex systems. However, models often involve uncertainty, which reduces their accuracy because of assumptions and simplifications made in a model's formulation. To improve the accuracy of a simulation in the presence of uncertainty, a probabilistic description of model prediction is desired. This strategy is useful for developing control algorithms, optimization techniques, and fault diagnosis tools for chemical processes as previously reported by others (Ma and Braatz, 2003; Mandur and Budman, 2014; Schenkendorf et al., 2019). The focus in this work is parametric uncertainty, and our objective is to quantify accurately how such an uncertainty impacts model prediction.

Uncertainty quantification (UQ) techniques are classified as either intrusive or nonintrusive approaches (Gel et al., 2013; Najm, 2009). For intrusive methods, which require modification of source code, stochastic models are developed from first principles of a system. In contrast, nonintrusive approaches rely on sampling techniques: deterministic models derived from first principles are iteratively executed with various sampling points of uncertainty (Gel et al., 2013). We present an intrusive UQ algorithm in this work and compare its UQ accuracy versus other intrusive and nonintrusive techniques using three cases: a benchmark nonlinear algebraic example, autocrine cell signalling networks, and a penicillin production process in chemical engineering.

For UQ, the intrusive generalized polynomial chaos (gPC) expansion is an extension of the polynomial chaos theory in the Wiener-Askey framework (Xiu and Karniadakis, 2002). For gPC, uncertainty is approximated by a random variable and its orthogonal polynomial basis functions. The parameters used to describe the relationship between the random variable and its polynomial basis functions are referred to as gPC coefficients. The resulting expression of uncertainty can then be substituted into a deterministic model to yield a stochastic model, from which the effect of uncertainty on model response can be predicted (Xiu, 2010). For intrusive gPC-based UQ, the formulation of stochastic models is based on a spectral representation in a random space, which is defined by random variables. In addition, the accuracy of UQ with

* Corresponding author.
E-mail address: ydu@clarkson.edu (Y. Du).

https://doi.org/10.1016/j.compchemeng.2019.106685
0098-1354/

gPC can be affected by the type of polynomial basis function used to approximate uncertainty. For example, in cases of normally distributed uncertainty Hermite polynomial basis functions are most appropriate (Eldred and Burkardt, 2009).

For intrusive gPC-based UQ, gPC coefficients of parametric uncertainty can be calculated with parameter estimation techniques such as maximum likelihood (Myung, 2003). However, the gPC coefficients of model predictions have to be calculated with a stochastic Galerkin (SG) projection to quantify the effect of uncertainty on model predictions. For SG, model predictions are projected against each polynomial basis function via an inner product, and each coefficient of model responses is extracted by the polynomial orthogonality property (Xiu, 2010). This generates a set of coupled models of gPC coefficients to describe the original stochastic system. Since the model has been changed with SG, the existing computer code to simulate the original system must be modified, which is why the SG-based UQ is classified as an intrusive method.

Although the literature reports that gPC-based UQ is an efficient approach (Xiu and Karniadakis, 2002), the SG projection poses great challenges, especially when the model involves nonpolynomial functions and when the number of uncertainties is large. This is because the inner product in the SG projection yields a high dimensional integral, which is difficult to solve in real-time (Debusschere et al., 2004). To address this issue, we previously used approximations to estimate high dimensional integrals in the SG projection with the bivariable dimension reduction method (Son and Du, 2019), which can deal with several uncertainties. Here we expand that work by presenting an intrusive UQ method that integrates a generalized dimension reduction with the SG projection to consider larger numbers of uncertainties (up to 10). Specifically, the generalized dimension reduction method (gDRM) (Xu and Rahman, 2004) is used to convert a high dimensional integral into several lower dimensional ones to calculate accurately gPC coefficients in a computationally efficient way.

Compared to intrusive UQ methods, nonintrusive techniques such as Monte Carlo (MC) simulations and its variants are methodically straightforward (Spanos and Zeldin, 1998). For MC, deterministic models are iteratively evaluated using different samples of uncertainty. Despite its simplicity, MC can be computationally demanding. Stochastic collocation (SC) is another powerful nonintrusive UQ tool based on the gPC theory. Like MC, SC is implemented by repeated simulations with different samples. Samples in SC are called collocation points, which are chosen based on sampling rules such as Lagrange polynomial interpolation or Gauss quadrature (Eldred and Burkardt, 2009; Xiu, 2007). The goal of SC-based UQ is to formulate a nodal set of collocation points in a random space. The simplest way is to use a tensor product that is based on the one-dimensional quadrature rule. However, use of a tensor product is not computationally efficient, especially when larger numbers of uncertainties are considered. In such cases, the number of collocation points grows exponentially as the number of uncertainties increases, which is the well-recognized curse of dimensionality. To reduce significantly the number of collocation points, a sparse grid-based sampling scheme constructed by the Smolyak algorithm following either Clenshaw–Curtis or Gaussian quadrature rules can be used (Xiu, 2010). Another way to generate collocation points is to use high-order unscented transformation (HOUT) (Julier and Uhlmann, 1997; Zhang et al., 2014). High-order unscented transformation was recently used to estimate uncertainties with different distributions, and its accuracy was verified with several examples (Xu and Dang, 2019).

The gPC-based UQ has been shown to be an efficient tool in different applications, including dynamic modelling, control, and optimization problems in chemical engineering (Duong et al., 2016; Najm, 2009; Shen and Braatz, 2016; Zhang and Sahinidis, 2013; Du et al., 2017). For example, the SC-based UQ was used for model predictive control design in a batch process to account for parametric and state uncertainties (Bradford and Imsland, 2019). The SG-based UQ method was used to improve simulation accuracy of a two-dimensional electrochemical microchannel flow (Debusschere et al., 2003). In process monitoring, gPC was used together with least-angle regression to optimally identify an auxiliary input to improve fault detection accuracy (Schenkendorf et al., 2019).

These successful applications suggest that the use of gPC-based UQ has much promise to improve process performance and safety in chemical engineering, but its broader use is likely limited by computational expense when larger numbers of uncertainties have to be considered in a nonlinear and complex system. Thus, to improve the computational efficiency of gPC-based UQ methods, we present a UQ method that integrates the gDRM with the gPC and report the detailed comparison between intrusive and nonintrusive UQ methods, which are discussed in Section 2 and Section 3, respectively. Our objective is to show the accuracy of the gDRM-based gPC approach when dealing with larger numbers of uncertainties in a nonlinear dynamic system, which is challenging for existing methods as others reported (Debusschere et al., 2004). Three cases are used for algorithm verification and presented in Section 4. Our conclusions are presented in Section 5.

2. Intrusive uncertainty quantification methods

2.1. Generalized polynomial chaos (gPC) expansion

For intrusive gPC-based UQ, uncertainty is generally approximated with a distribution using a predefined probability density function (PDF) of another random variable (e.g., ξ); a set of coupled equations of gPC coefficients are used to provide a probabilistic description of model outputs. Assume a system can be defined with (ordinary) differential equations (ODEs) over a period of time ($T > t_0$) as in Xiu (2010):

$$\dot{\boldsymbol{u}} = \boldsymbol{g}\left(t, \boldsymbol{u}, \boldsymbol{\theta}, \boldsymbol{\rho}\right), \ t \in (t_0, T] \tag{1}$$

where $\boldsymbol{g}$ are nonlinear functions, $\boldsymbol{u} = (u_{j=1}, \ \ldots, u_{j=J}) \in \mathbb{R}^J$ are model responses (or outputs) over a given time domain (t_0,T] with initial values of $\boldsymbol{u}_0$ at $t = t_0$, and $J \geq 1$, $\boldsymbol{\theta}$ define deterministic model parameters that are fixed constants, $\boldsymbol{\rho}$ are uncertain parameters where $\boldsymbol{\rho} = (\rho_1, \ \ldots, \ \rho_N) \in \mathbb{R}^N$, and N (≥ 1) is the number of parametric uncertainties. In this work, the parameters in $\boldsymbol{\rho}$ are independent and identically distributed, and each of which can be described with a PDF following a predefined distribution.

To quantify the effect of uncertainty on $\boldsymbol{u}$, the first step is to approximate each parameter ρ_i (i = 1, 2, ..., N) in $\boldsymbol{\rho}$ with a random variable ξ_i as in Xiu (2010):

$$\rho_i = \rho_i(\xi_i) = \sum_{n=0}^{\infty} \hat{\rho}_{i,n} \ \psi_n(\xi_i) \approx \sum_{n=0}^{P} \hat{\rho}_{i,n} \psi_n(\xi_i) \tag{2}$$

where $\{\hat{\rho}_{i,n}\}$ are the gPC coefficients used to approximate the i^{th} parametric uncertainty, and $\{\psi_n(\xi_i)\}$ are the polynomial basis functions depending on the PDF of ρ_i. Importantly, the orthogonal polynomial basis functions must be appropriately selected with respect to the PDF of ρ_i. Some frequently used basis functions can be found in Eldred and Burkardt (2009), Xiu (2010).

Since parametric uncertainty affects model responses, each model output u_j is approximated with random variables $\boldsymbol{\xi} = (\xi_1, \cdots, \xi_i, \cdots, \xi_N)$ that are used to approximate $\{\rho_i\}$, which can be described as in Xiu (2010):

$$u_j\left(t, \boldsymbol{\xi}\right) = \sum_{m=0}^{\infty} \hat{u}_{j,m}(t) \Psi_m\left(\boldsymbol{\xi}\right) \approx \sum_{m=0}^{\mathrm{M}} \hat{u}_{j,m}(t) \Psi_m\left(\boldsymbol{\xi}\right) \tag{3}$$

where $\{\hat{u}_{j,m}\}$ are the gPC coefficients of the j^{th} output at time t, and $\Psi_m(\boldsymbol{\xi})$ is a multivariate polynomial basis function calculated with $\psi_n(\xi_i)$ as follows (Eldred and Burkardt, 2009):

$$\Psi_m(\boldsymbol{\xi}) = \prod_{i=0}^{N} \psi_{d_i^m}(\xi_i) \tag{4}$$

where d_i^m is an index of basis function. For instance, when a two-dimensional random space having two parametric uncertainties is considered ($i = 1$ and 2), then $d_1^1 = 1$ and $d_2^1 = 0$ with $m = 1$. Details about the calculation of $\Psi_m(\boldsymbol{\xi})$ can be found in Eldred and Burkardt (2009).

For practical applications, a finite number of terms as seen in (2) and (3), $P+1$ and $M+1$ (including a zeroth term) are used in gPC expansions instead of an infinite number of terms. Note that P in (2) is also called as polynomial order, which is selected such that *a priori* PDF of uncertainty can be optimally approximated following the gPC theory. The total number of terms of u_j in (3) (i.e., $M+1$) is calculated as (5), which is a function of P and the total number of uncertainties N (Debusschere et al., 2004; Xiu, 2010).

$$M+1 = \binom{N+P}{N} = \frac{(N+P)!}{P!N!} \tag{5}$$

Unlike the gPC expansions of ρ_i, which can be determined with *prior* knowledge or offline calibration, the gPC coefficients of u_j in (3) (e.g., $\hat{u}_{j,m}(t)$) have to be calculated by substituting (2) and (3) into (1), and subsequently by using an SG projection as in Xiu (2010):

$$\langle \dot{u}_j(t,\boldsymbol{\xi}), \Psi_m(\boldsymbol{\xi}) \rangle = \langle \boldsymbol{g}(t, u_j(t,\boldsymbol{\xi}), \boldsymbol{\theta}, \boldsymbol{\rho}(\boldsymbol{\xi})), \Psi_m(\boldsymbol{\xi}) \rangle \tag{6}$$

where $\langle \cdot \rangle$ is the inner product operator. Following (6), (1) is then converted into a family of coupled models of gPC coefficients $\{\hat{u}_{j,m}\}$. The inner product between any two vectors in (6) is calculated as in Xiu (2010):

$$\langle \phi(\boldsymbol{\xi}), \phi'(\boldsymbol{\xi}) \rangle = \int_{\mathbb{R}^N} \phi(\boldsymbol{\xi}) \phi'(\boldsymbol{\xi}) W(\boldsymbol{\xi}) d\boldsymbol{\xi} \tag{7}$$

where the multi-dimensional integral is calculated over the domain $\mathbb{R}^N$ defined by random variables $\boldsymbol{\xi}$, and $W(\boldsymbol{\xi})$ is the weight function (i.e., the joint PDF of random variables $\boldsymbol{\xi}$).

The gPC coefficients of $\boldsymbol{u}$ can be used to predict statistical moments of model outputs at any given time point t. For example, the first and second moments, the mean and variance of the j^{th} output u_j, can be calculated as in Debusschere et al. (2003), Xiu (2010):

$$E[u_j(t)] = E\left[\sum_{m=0}^{M} \hat{u}_{j,m}(t)\Psi_m\right] = \hat{u}_{j,0}(t)E[\Psi_0] + \sum_{m=1}^{M} \hat{u}_{j,m}(t)E[\Psi_m] = \hat{u}_{j,0}(t) \tag{8}$$

$$\begin{aligned} Var[u_j(t)] &= E\left[\left\{u_j(t) - E[u_j(t)]\right\}^2\right] \\ &= E\left[\left\{\sum_{m=0}^{M} \hat{u}_{j,m}(t)\Psi_m - \hat{u}_{j,0}(t)\right\}^2\right] \\ &= E\left[\left\{\sum_{m=1}^{M} \hat{u}_{j,m}(t)\Psi_m\right\}^2\right] = \sum_{m=1}^{M} \{\hat{u}_{j,m}(t)\}^2 E[\Psi_m^2] \end{aligned} \tag{9}$$

where $E[\cdot]$ denotes expectation. As seen in (8) and (9), the mean of u_j can be estimated with the first gPC coefficient $\hat{u}_{j,m=0}$, while the variance of u_j is approximated using other higher-order gPC coefficients $\hat{u}_{j,m\neq 0}$ and the expectation of Ψ_m^2 (Debusschere et al., 2003; Xiu, 2010).

2.2. Stochastic Galerkin (SG) projection based on dimension reduction

The calculation of gPC coefficients $\{\hat{u}_{j,m}\}$ with the SG projection can be computationally prohibitive or even impossible, when non-polynomial functions appear as in (1) (Debusschere et al., 2004). To address this, in this work we combine the gDRM (Xu and Rahman, 2004) with the gPC theory. Following the SG procedure, the calculation of gPC coefficients $\{\hat{u}_{j,m}\}$ of u_j in (3) can be defined with an integral as in Xiu (2010):

$$\hat{u}_{j,m}(t) := \frac{1}{\gamma_m} \int_{\mathbb{R}^N} u_j(t,\boldsymbol{\xi}) \Psi_m(\boldsymbol{\xi}) W(\boldsymbol{\xi}) d\boldsymbol{\xi} \tag{10}$$

where γ_m is the expectation of the square of the polynomial basis function Ψ_m, $\gamma_m = E[\Psi_m^2]$. To quickly calculate gPC coefficients of u_j, the gDRM is used to estimate the high-dimensional integral in (10) with several lower dimensional ones (e.g., one-, two-, and three-dimensional integrals).

Let us define $y(\boldsymbol{\xi})$ at a particular time point t in (10) as $y(\boldsymbol{\xi}) = u_j(t,\boldsymbol{\xi})\Psi_m(\boldsymbol{\xi})$, which is a continuous, differentiable, and real-valued function. Following this, the integral in (10) can be rewritten as in Xu and Rahman (2004):

$$E[y(\boldsymbol{\xi})] = \int_{\mathbb{R}^N} y(\boldsymbol{\xi}) W(\boldsymbol{\xi}) d\boldsymbol{\xi} \tag{11}$$

Following the definition of gDRM, $y(\boldsymbol{\xi})$ is estimated with an S-variate approximation as in Xu and Rahman (2004):

$$\hat{y}(\boldsymbol{\xi}) = \sum_{r=0}^{S} (-1)^r \binom{N-S+r-1}{r} y_{S-r}, \quad S \leq N \tag{12}$$

where S is an index defining the maximum number of random variables in the N-dimensional random space. These random variables will define a new subdomain to approximate $y(\boldsymbol{\xi})$ and $S \ll N$. For example, when S is 2, the N-dimensional integral is converted into several one- and two-dimensional integrals. In this work, we focus on two cases, $S = 2$ and $S = 3$, hereafter referred to as bivariable dimension reduction method (BiDRM) and trivariable dimension reduction method (TriDRM), respectively. However, it is important to note that a larger value of S (> 3) can be used to improve UQ accuracy.

Based on the definition of gDRM, each term y_{S-r} in (12) is defined as in Xu and Rahman (2004):

$$y_{S-r} = \sum_{l_1 < l_2 < \cdots < l_{S-r}} y(0,\ldots,0,\xi_{l_1},0,\ldots,0,\xi_{l_2},0,\ldots,0,\xi_{l_{S-r}},0) \tag{13}$$

where $l_1, l_2, \ldots, l_{S-r} \in \{1, 2, \ldots, N\}$, and $y_0 = y(\mathbf{0})$ by assigning all variables in $\boldsymbol{\xi}$ to 0. Thus, the mean value of $\hat{y}(\boldsymbol{\xi})$ can be defined as in Huang and Du (2006), Xu and Rahman (2004):

$$E[\hat{y}(\boldsymbol{\xi})] = \sum_{r=0}^{S} (-1)^r \binom{N-S+r-1}{r} E[y_{S-r}] \tag{14}$$

where $E[y_{S-r}]$ is a lower-dimensional integral used to estimate $E[y(\boldsymbol{\xi})]$. For example, in TriDRM when S is 3, each term $E[y_{S-r}]$ in (14) can be defined as in Huang and Du (2006), Xu and Rahman (2004):

$$E[y_0] = y(\mathbf{0}) = y_0 = y(0,\ldots,0) \tag{15}$$

$$E[y_1] = \sum_{l} E[y(0,\ldots,0,\xi_l,0,\ldots,0)], \quad l = 1,\ldots,N \tag{16}$$

$$E[y_2] = \sum_{l_1 < l_2} E[y(0,\ldots,0,\xi_{l_1},0,\ldots,0,\xi_{l_2},0,\ldots,0)] \tag{17}$$

$$E[y_3] = \sum_{l_1 < l_2 < l_3} E[y(0,\ldots,0,\xi_{l_1},0,\ldots,0,\xi_{l_2},0,\ldots,0,\xi_{l_3},0)] \tag{18}$$

where each term involves at most three random variables of $\boldsymbol{\xi}$ in (3) to approximate uncertainty. For instance, $y(\mathbf{0})$ in (15) is calculated by setting $\boldsymbol{\xi}$ to 0, and (16) through (18) are calculated with summations of integrals involving one-, two-, and three-random variables, respectively. Examples of different integrations in (16) to (18) are shown as follows (Xu and Rahman, 2004).

$$E[y(0,\ldots,0,\xi_l,0,\ \ldots,0)]\equiv\int_{-\infty}^{\infty}y(0,\ldots,0,\xi_l,0,\ \ldots,0)W(\xi_l)d\xi_l \tag{19}$$

$$E\left[y\left(0,\ldots,0,\xi_{l_1},0,\ldots,0,\xi_{l_2},0,\ldots,0\right)\right] \equiv\int_{-\infty}^{\infty}y\left(0,\ldots,0,\xi_{l_1},0,\ldots,0,\xi_{l_2},0,\ldots,0\right)W\left(\bar{\boldsymbol{\xi}}\right)d\bar{\boldsymbol{\xi}} \tag{20}$$

$$E\left[y\left(0,\ldots,0,\xi_{l_1},0,\ldots,0,\xi_{l_2},0,\ldots,0,\xi_{l_3},0\right)\right] \equiv\int_{-\infty}^{\infty}y\left(0,\ldots,0,\xi_{l_1},0,\ldots,0,\xi_{l_2},0,\ldots,0,\xi_{l_3},0\right)W\left(\bar{\boldsymbol{\xi}}\right)d\bar{\boldsymbol{\xi}} \tag{21}$$

where $\bar{\boldsymbol{\xi}}$ is a subdomain of $\boldsymbol{\xi}$, (i.e., $\bar{\boldsymbol{\xi}}=\{\xi_{l_1},\ \xi_{l_2}\}$ in (20) and $\bar{\boldsymbol{\xi}}=\{\xi_{l_1},\ \xi_{l_2},\ \xi_{l_3}\}$ in (21)) and $W(\bar{\boldsymbol{\xi}})$ is the joint PDF of $\bar{\boldsymbol{\xi}}$. Notably, $E[y_1]$ is approximated with a summation of N different one-dimensional integrals, whereas $E[y_2]$ and $E[y_3]$ are calculated using summations of $\binom{N}{2}$ two- and $\binom{N}{3}$ three-dimensional integrals, respectively.

Using the approximation of a high dimensional integral as shown in (14), the gPC coefficients in (10) can be calculated as:

$$\hat{u}_{j,m}(t)\cong\frac{1}{\gamma_m}E\left[\hat{y}\left(\boldsymbol{\xi}\right)\right]=\frac{1}{\gamma_m}\sum_{r=0}^{S}(-1)^r\binom{N-S+r-1}{r}E[y_{S-r}] \tag{22}$$

where $E[y_{S-r}]$ is calculated following (15) through (18).

Therefore, using the gDRM, the difficulty to calculate a high-dimensional integral involved in the SG projection (e.g., $E[y(\boldsymbol{\xi})]$ in (11)) can be alleviated by calculating a few lower-dimensional integrals. To illustrate UQ accuracy of the proposed algorithm, BiDRM- and TriDRM-based SG projections are used in this work; results are compared to other nonintrusive techniques including Monte Carlo simulations, stochastic collocation, and a recently developed high-order unscented transformation method (Julier and Uhlmann, 1997; Xu and Dang, 2019; Zhang et al., 2014).

3. Nonintrusive uncertainty quantification methods

3.1. Stochastic collocation (SC)

Compared to intrusive SG, nonintrusive stochastic collocation (SC) is straightforward. Its implementation is methodologically similar to MC (Xiu, 2007). Details about SC can be found in Eldred and Burkardt (2009), Xiu (2010). To approximate uncertainty in the model's output u_j, which results from parametric uncertainties in the model, the following gPC expansions are defined (Xiu, 2010, 2007):

$$u_j\approx v_j\left(t,\boldsymbol{\xi}\right)=\sum_{m=0}^{\mathrm{M}}\hat{v}_{j,m}(t)\Psi_m\left(\boldsymbol{\xi}\right) \tag{23}$$

$$\hat{v}_{j,m}(t)\ =\ \frac{1}{\gamma_m}\sum_{k=1}^{\mathrm{Q}}u_j\left(t,\boldsymbol{p}^k\right)\Psi_m\left(\boldsymbol{p}^k\right)\alpha^k \tag{24}$$

where $v_j(t,\boldsymbol{\xi})$ in (23) is the gPC approximation of u_j and the total number of terms in (23), $M+1$ (including zeroth term), can be calculated with (5). In (24), Q is the total number of nodal points used to approximate gPC coefficients, and $\{\boldsymbol{p}^k,\alpha^k\}_{k=1}^{Q}$ denotes a set of nodes and weights. Here, $\boldsymbol{p}^k=(p_1^k,\ \ldots,\ p_N^k)$ is the k^{th} set of nodes in a random space defined by N random variables, and its corresponding weight is defined as α^k.

To calculate gPC coefficients, $\hat{v}_{j,m}$ in (24), an interpolating operator to construct quadrature rules is defined as below (Xiu, 2010, 2007):

$$\mathcal{U}^{Q}\equiv\sum_{k=1}^{Q}f\left(\boldsymbol{p}^k\right)\alpha^k\cong\int f\left(\boldsymbol{\xi}\right)W\left(\boldsymbol{\xi}\right)\mathrm{d}\boldsymbol{\xi} \tag{25}$$

$$f\left(\boldsymbol{p}^k\right)=u_j(\mathrm{t},\ \boldsymbol{p}^k)\Psi_m\left(\boldsymbol{p}^k\right) \tag{26}$$

Importantly, the nodal set in (25), $\{\boldsymbol{p}^k,\alpha^k\}_{k=1}^{Q}$, must be appropriately selected to ensure the accuracy of the integral in (25). (among the rules available to optimally select a nodal set, Gauss quadrature rules are often used due to their simplicity.) Each point and its corresponding weight in the nodal set may also be referred to as collocation points. For each random variable, a one-dimensional quadrature operator can be constructed as in Xiu (2010, 2007):

$$\mathcal{U}_i^{q_i}\equiv\sum_{k=1}^{q_i}f\left(p_i^k\right)\alpha_i^k \tag{27}$$

where i is the i^{th} random variable, and the nodal sets used in (27) can be given as in Xiu (2007):

$$\boldsymbol{\Theta}_i^1=\left(p_i^1,\ldots,p_i^{q_i}\right)\subset\Gamma_i \tag{28}$$

where Γ_i is a random space of the i^{th} random variable such that $\Gamma\equiv\prod_{i=1}^{N}\Gamma_i\subset\mathbb{R}^N$ (Xiu, 2007). To generate collocation points for a multidimensional random variable space, two approximations are available: use of a full tensor product grid or a sparse grid with a smaller number of collocation points, discussed below.

3.1.1. Tensor products

The easiest way to approximate a high-dimensional integral is a full tensor product, which consists of one-dimensional integration rules for each random variable and can be defined as (Xiu, 2007):

$$\begin{aligned}\mathcal{U}^{Q}[f]&\equiv\left(\mathcal{U}_i^{q_i}\otimes\cdots\otimes\mathcal{U}_N^{q_N}\right)[f]\\&=\sum_{k_1=1}^{q_1}\cdots\sum_{k_N=1}^{q_N}f\left(p_1^{k_1},\cdots,p_N^{k_N}\right)\cdot\left(\alpha_1^{k_1}\otimes\cdots\otimes\alpha_N^{k_N}\right)\end{aligned} \tag{29}$$

The total number of points, Q in (29), can be calculated as $Q=\prod_{i=1}^{N}q_i$, where q_i is the number of nodal sets used for each variable. Thus, as the number of random variables increases, the total number of collocation points also increases exponentially. In this case, a sparse grid using the Smolyak algorithm can be used to reduce the number of collocation points.

3.1.2. Sparse grids

The sparse grid method is computationally efficient for high dimensional problems. It uses linear combinations of carefully selected tensor products to preserve the interpolation property for a high-dimensional random space (Judd et al., 2014). To estimate a multidimensional integral, the sparse grid formula can be defined as in Nobile et al. (2008), Xiu (2007):

$$\begin{aligned}\mathcal{U}^{Q}(f)\equiv\mathcal{A}(w,N)=&\sum_{w+1\le|i|\le w+N}(-1)^{w+N-|i|}\cdot\binom{N-1}{w+N-|i|}\\&\cdot\left(\mathcal{U}_{i_1}\otimes\cdots\otimes\mathcal{U}_{i_N}\right)\end{aligned} \tag{30}$$

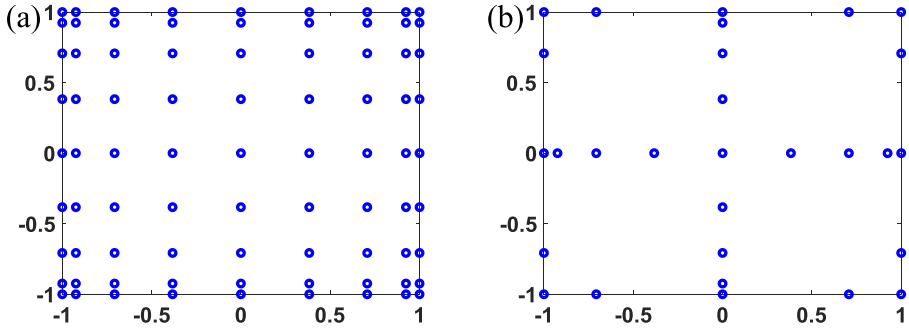

Fig. 1. Illustration of collocation points for two-dimensional space ($N = 2$) with an approximation level $w = 3$ (Eldred and Burkardt, 2009). (a) full tensor product grid and (b) Smolyak sparse grid from the extrema of Chebyshev polynomials (Clenshaw-Curtis quadrature).

where $|i| = i_1 + \cdots + i_N$, N is the total number of uncertainties, and w is an approximation level that controls the number of elements in the tensor product involved in the Smolyak grid. As the approximation level increases, the quality of approximation is improved by increasing the number of collocation points (Judd al., 2014). The isotropic Smolyak method is used in this work to calculate $\mathcal{A}(w, N)$ in (30) for simplicity. To calculate $\mathcal{A}(w, N)$, the function value f defined in (26) must be computed. This can be estimated with sparse grid points used in (30), $\mathcal{H}(w, N)$, which is defined as in Xiu (2007):

$$\boldsymbol{\Theta}_N \equiv \mathcal{H}(w, N) = \underset{w+1\le|i|\le w+N}{\cup} \left(\boldsymbol{\Theta}^1_{i_1} \times \cdots \times \boldsymbol{\Theta}^1_{i_N}\right) \tag{31}$$

Note that when nodal sets of each dimension are nested, such that $\boldsymbol{\Theta}^1_{i,w} \subset \boldsymbol{\Theta}^1_{i,w+1}$, the total number of nodal sets in (31) can be significantly reduced since $\mathcal{H}(w, N) \subset \mathcal{H}(w+1, N)$. Details to calculate a set of nodes and their corresponding weights in the sparse grid can be found in Judd et al. (2014), Smolyak (1963). In this work, the isotropic Smolyak algorithm is used to construct sparse grids using the most popular Clenshaw-Curtis and the Gaussian-Hermite quadrature rules, but other approaches can be also considered (Eldred and Burkardt, 2009).

To illustrate the use of the Clenshaw-Curtis quadrature, Fig. 1 shows collocation points of a two-dimensional space with two random variables, when the full tensor product and the Smolyak algorithm were used to generate the nodal points with the same approximation level w. The sparse grid significantly reduces the number of collocation points, compared to the full tensor grid. The implementation of SC with sparse grids is discussed in Section 4.

3.1.3. High-order unscented transformation

Another SC-based UQ approach is the unscented transformation (UT) whose members of the nodal set are often referred to as sigma points. Since UT only requires $2N+1$ sigma points, which may fail to provide an accurate estimation of high-order statistical moments (Wang and Cheng, 2015; Xiao and Lu, 2018), a high-order unscented transformation (HOUT) was recently developed using $2N^2+1$ sigma points to estimate the high-order statistical moments of random variables (Julier and Uhlmann, 1997; Xiao and Lu, 2018; Xu and Dang, 2019; Zhang et al., 2014). The HOUT is also used in this work to compare UQ accuracy.

Critical to HOUT is the appropriate selection of three classes of sigma points. As an example, Fig. 2 shows sigma points required for a two-dimensional random space (N =2). The first class has a single point s_0, lying at the origin with a weight of Ω_0. For the second class, there are $2N$ points located on the coordinates, which have identical distance s_1 from the origin and a weight of Ω_1. The third class consists of $2N(N-1)$ points, which lie at (0, ..., $\pm s_2$, ..., $\pm s_2$, ...,0) and a weight of Ω_2. Notably, sigma points in the second class only have one nonzero element, (0, ..., $\pm s_1$, ..., 0), while sigma points in the third class have two nonzero elements

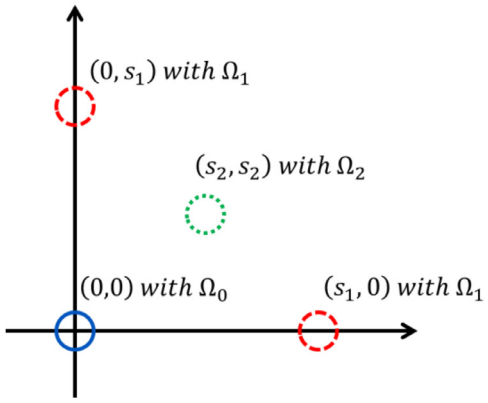

Fig. 2. Illustration of sigma points for two-dimensional space involved in HOUT: The blue circle at the origin represents the first class of sigma points, the red circles represent the second class of sigma points, and the green circle represents the third class of sigma points (Zhang et al., 2014).

in the random space (Cheng et al., 2016; Xu and Dang, 2019). In addition, the total number of sigma points can be calculated as $2N(N-1)+2N+1 = 2N^2+1$. Details of HOUT can be found in Cheng et al., 2016, Xiao and Lu (2018), Zhang et al. (2014), but three types of sigma points and their corresponding weights are given as follows for clarity.

Class 1:

$$\bar{\boldsymbol{s}}_0 = 0, \quad \Omega_0 = \frac{-2N^2 + (4-2N)\beta^2 + (4\beta+4)N}{\left(N+\beta^2\right)(4-N)} \tag{32}$$

Class 2:

$$\begin{cases} \bar{\boldsymbol{s}}_{\omega_1} = +\sqrt{\dfrac{(4-N)(N+\beta)}{(\beta+2-N)}}\boldsymbol{e}_{\omega_1} \\ \bar{\boldsymbol{s}}_{\omega_1+N} = -\sqrt{\dfrac{(4-N)(N+\beta)}{(\beta+2-N)}}\boldsymbol{e}_{\omega_1} \end{cases} \tag{33}$$

$$\Omega_1 = \frac{(\beta+2-N)^2}{2(N+\beta)^2(4-N)} \tag{34}$$

where $\omega_1 = 1, 2, \ldots, N$, and $\boldsymbol{e}_{\omega_1}$ has 1 at the ω_1 element, $\boldsymbol{e}_{\omega_1} = [0, \ldots, 0, 1, 0, \ldots 0]^T$.

Class 3:

$$\begin{cases} \bar{\boldsymbol{s}}_{\omega_2} = +\sqrt{(n+\beta)}\boldsymbol{s}^+_{\omega_2} \\ \bar{\boldsymbol{s}}_{\omega_2+0.5N(N-1)} = -\sqrt{(n+\beta)}\boldsymbol{s}^+_{\omega_2} \\ \bar{\boldsymbol{s}}_{\omega_2+N(N-1)} = +\sqrt{(n+\beta)}\boldsymbol{s}^-_{\omega_2} \\ \bar{\boldsymbol{s}}_{\omega_2+1.5N(N-1)} = -\sqrt{(n+\beta)}\boldsymbol{s}^-_{\omega_2} \end{cases} \tag{35}$$

$$\Omega_2 = \frac{1}{(N+\beta)^2} \tag{36}$$

where $\omega_2 = 1,\ 2,\ \ldots,\ 0.5N(N-1)$, and $\boldsymbol{s}^+_{\omega_2}$ and $\boldsymbol{s}^-_{\omega_2}$ are given as below:

$$\boldsymbol{s}^+_{\omega_2} = \left\{ \sqrt{\frac{1}{2}}(\boldsymbol{e}_\kappa + \boldsymbol{e}_\lambda) : \kappa < \lambda,\ \kappa,\ \lambda = 1,\ 2,\ \ldots,\ N \right\} \tag{37}$$

$$\boldsymbol{s}^-_{\omega_2} = \left\{ \sqrt{\frac{1}{2}}(\boldsymbol{e}_\kappa - \boldsymbol{e}_\lambda) : \kappa < \lambda,\ \kappa,\ \lambda = 1,\ 2,\ \ldots,\ N \right\} \tag{38}$$

The free parameter β in (32) through (36) is a problem-specific value used to ensure UQ accuracy. For example, it can be set to 0.835 and 1.417, when the number of uncertainties is 2 and 3, respectively; otherwise, β can be set to 2. Details for calculating β can be found in Xiao and Lu (2018), Zhang et al. (2014).

3.2. Monte Carlo simulations

Monte Carlo (MC) simulations are the most frequently used method for UQ (Spanos and Zeldin, 1998). However, it requires repeated executions of deterministic models with different samples, which increase computational burden, especially when the number of uncertainties is large. However, since the convergence of MC is unaffected by the dimension of uncertainties (Xiu and Hesthaven, 2005), in this work we use MC simulation as a benchmark for comparison of different UQ techniques' accuracy.

4. Implementation of numerical examples

Three case studies were chosen here to compare the performance of different intrusive and nonintrusive UQ methods in terms of UQ accuracy. A nonlinear algebraic example was first used as a benchmark test to compare the accuracy of gDRM-based gPC algorithm (BiDRM and TriDRM) to several other existing methods. Two examples in chemical engineering, a penicillin manufacturing process, and living-cell signalling networks, were selected to show both accuracy and computing efficiency of the gDRM-based gPC for UQ when dealing with nonlinear and complex systems that involve larger numbers of uncertainties (up to 10). Since MC is the most common technique and generally provides good UQ results, it was chosen as a reference to verify the accuracy of other intrusive and nonintrusive techniques.

4.1. Case 1: nonlinear algebraic problem

The accuracy of different UQ methods is first compared using a nonlinear algebraic case, for which the model response, Z, can be defined as in Xiu (2007), Xu and Rahman (2004):

$$Z = \sqrt{1 + 0.5\boldsymbol{X}\boldsymbol{X}^T} \ln\left(\frac{1}{2} + \boldsymbol{X}\boldsymbol{X}^T\right) \tag{39}$$

where $\boldsymbol{X}$ is a vector defining N parametric uncertainties, X_i (i = 1, ..., N). We assume that uncertainties in $\boldsymbol{X}$ are independent and identically distributed and follow a normal distribution with a mean value of μ_x and a variance of ${\sigma_x}^2$. Two mean values of $\{X_i\}$ were used (0 and 1) as were several values of σ_x of $\boldsymbol{X}$ (See Fig. 3) to demonstrate how UQ accuracy of different UQ methods can be affected by the magnitude of uncertainty. Since uncertainty in $\boldsymbol{X}$ follows a normal distribution, Hermite polynomials were used as polynomial basis functions for SG- and SC-based UQ. To show UQ accuracy, N was set to 4 in (39). To quantify UQ accuracy, the relative error of the mean value of Z was used and calculated as:

$$\epsilon_\mu = \left| \frac{\mu_r - \mu}{\mu} \right| \tag{40}$$

where μ is the predicted model response evaluated with (39) using the mean values of $\boldsymbol{X}$, and μ_r is the mean value of Z calculated with different methods, including BiDRM- and TriDRM-based SG, nonintrusive SC, and MC simulations.

4.1.1. Results of case 1 - Nonlinear algebraic benchmark

For intrusive UQ methods, BiDRM and TriDRM were used to convert a high-dimensional integral in the SG projection into several lower dimensional ones. The calculation of gPC coefficients of Z followed the procedures described in Section 2. The BiDRM-based SG converts the N-dimensional integral into N one-dimensional and $\binom{N}{2}$ two-dimensional ones. While the TriDRM-based SG converts the high dimensional integral into N one-dimensional, $\binom{N}{2}$ two-dimensional, and $\binom{N}{3}$ three-dimensional ones. Once the gPC coefficients of Z were determined, the mean and variance of Z were estimated using (8) and (9).

To demonstrate the efficiency of the gDRM-based UQ, the trapezoidal rule was also used in this case to estimate the high-dimensional integrals in SG. The trapezoidal rule is one of the most common and simplest techniques to approximate a numerical integration. This is achieved by dividing the integral domain into several small and equal segments called trapezoids, and evaluating the integrand at each subinterval, followed by a summation of estimates (Hill and Moore, 2004; Yeh, 2002). In this case study, the number of subintervals in each dimension was set to 100.

For nonintrusive UQ, we used a full tensor grid (SC-FT) and a sparse grid (SC-SP). The full tensor grid was constructed based on one-dimensional Gauss-Hermite quadrature rules, which has the same number of collocation points for each uncertainty, $q = 5$. Since the total number of collocation points in the full grid can be defined as $Q = q^N$ and N was set to 4, 5^4 collocation points were required in total for the full tensor grid points based UQ.

For SC-SP, the Smolyak algorithm with the Gauss-Hermite quadrature was used to construct collocation points for two different approximation levels, $w = 3$ and 5, to show the effect of approximation levels on UQ accuracy. When w was set to 3, 289 grid points were required and when w was 5, 4994 grid points were needed. The sigma points-based HOUT was also used for comparison among different nonintrusive UQ methods. Since the total number of sigma points associated with the dimension of uncertainties is $Q = 2N^2 + 1$, 33 points in total were required, an amount significantly lower than other SC-based methods. Further, 10^6 samples were used for MC; its results were used as the reference benchmark to compare UQ accuracy.

Fig. 3 shows the UQ results using different methods, where the first row and the second row of graphs show the results of Z, when the mean value of X_i was 1 and 0, respectively. Also, for comparison purposes, the standard deviation σ_x was varied from 0.05 to 0.7. For different mean values of $\boldsymbol{X}$, the first column in Fig. 3 shows the relative error of Z. As seen, all methods provide accurate UQ results as compared to MC, when uncertainty is small (e.g., when σ_x is less than 0.5). In addition, we found that the UQ accuracy can be affected by uncertainty, especially when the mean value of uncertainty is smaller.

Further, the variance in Z, resulting from uncertainty in $\boldsymbol{X}$, is also calculated and shown in the second column of Fig. 3 for comparison. As seen, the accuracy of the variance in Z with different methods can be affected by uncertainty in $\boldsymbol{X}$. For example, as seen in Fig. 3(d), the discrepancy between BiDRM-based SG and MC becomes larger, as uncertainty (σ_x) increases, when the mean value is 0. It is also important to note that the discrepancy can be eliminated, when TriDRM is used. Specifically, as seen in Fig. 3(c) and (d), the intrusive TriDRM-based UQ method provides results as accurate as other nonintrusive methods. This clearly shows the potential of the gDRM-based SG for dealing with higher dimensional problems that involve nonpolynomial functions, which was previously found challenging with intrusive gPC-based UQ (Debusschere et al., 2004). Based on this, the efficiency

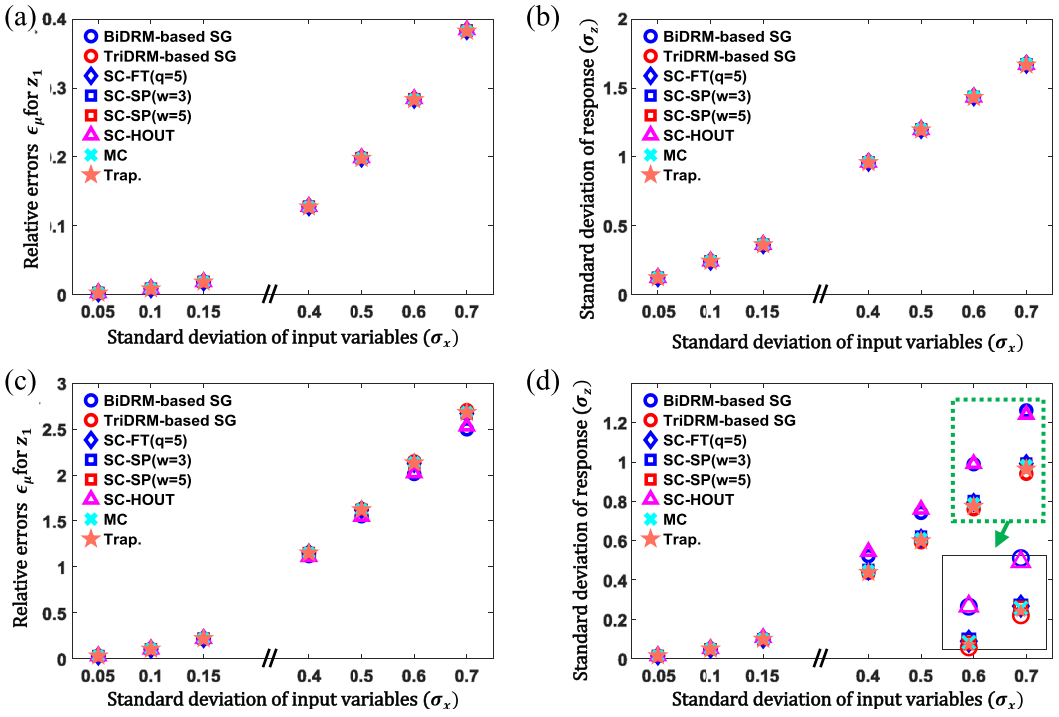

Fig. 3. Comparison of relative errors ϵ_μ and standard deviations σ_z of Z. For (a) and (b), the mean value of $\{X_i\}$ was set to 1, while the mean value of $\{X_i\}$ was set to 0 in (c) and (d). Note that "Trap." here represents the trapezoidal rules-based UQ method.

of the gDRM-based SG method in terms of UQ accuracy will be further discussed in case studies 2 and 3 below.

As compared to the intrusive UQ method, we found that the accuracy of the nonintrusive SC methods can be affected by the number of collocation points and/or the approximation levels. For example, the difference of relative errors between the SC-SP constructed by the Smolyak algorithm and MC is smaller when w is 5, as compared to the case where w is 3. Also as seen in Fig. 3, trapezoidal rules can provide accurate UQ results, when they were used to estimate the integral involved in SG projection. However, it is important to note that when the number of uncertainties increases (e.g., $N = 10$ in this work discussed later), we found that the total number of nodes required to estimate the integral in the SG becomes significantly large with trapezoidal rules. For example, when the number of uncertainties is 10 and when 10 discretised subintervals in each dimension are used, the total number of points required to approximate an integral involved in SG is $(10+1)^{10}$ (Hill and Moore, 2004), which is time prohibitive for solving gPC coefficients. This is also the reason that a smaller number of uncertainties, $N = 4$, is considered in this benchmark test, since our main objective here is to show and compare the accuracy of different methods.

4.2. Case 2: fed-batch penicillin manufacturing process

In the second case study, a fed-batch penicillin production process is used to demonstrate the computing efficiency of the proposed intrusive UQ method. In this case, a modified model developed in Birol et al. (2002) is used. Notably, we assumed that temperature and pH value remained unchanged, and oxygen was not limiting (Mandur and Budman, 2014). The model consists of substrate, biomass, and penicillin concentrations, which is described as in Bajpai and Reuß (1980), Birol et al. (2002), Mandur and Budman (2014):

$$\frac{dC_X}{dt} = \left(\frac{\mu_X C_S C_X}{K_X C_X + C_S}\right) - \frac{C_X}{V}\frac{dV}{dt} \tag{41}$$

$$\frac{dC_P}{dt} = \left(\frac{\mu_P C_S C_X}{K_P + C_S + \frac{C_S^2}{K_I}}\right) - K_H C_P - \frac{C_P}{V}\frac{dV}{dt} \tag{42}$$

$$\frac{dC_S}{dt} = -\left(\frac{1}{Y_{X/S}}\frac{\mu_X C_S C_X}{K_X C_X + C_S}\right) - \left(\frac{1}{Y_{P/S}}\frac{\mu_P C_S C_X}{K_P + C_S + \frac{C_S^2}{K_I}}\right) - m_X C_X + \frac{F s_f}{V} - \frac{C_S}{V}\frac{dV}{dt} \tag{43}$$

$$\frac{dV}{dt} = F - 6.226 \times 10^{-4} V \tag{44}$$

where C_X, C_P, and C_S are the concentrations of biomass, penicillin, and substrate, respectively; and V is the culture volume. The description and values of model parameters can be found in previous work (Bajpai and Reuß, 1980; Birol et al., 2002; Mandur and Budman, 2014).

To better evaluate the effect of uncertainty in model parameters on the penicillin production, we first used the half-norm graph-based sensitivity analysis method developed in our previous work (Son et al., 2018), which is not discussed further for brevity. The effect of parameters on model responses can be described as following in descending order: $\mu_P > s_f > F > K_H > \mu_x > Y_{X/S} > K_I > K_X > m_x > Y_{P/S} > K_P$. Using this, different numbers of parametric uncertainties were considered to show the efficiency of the proposed UQ method for dealing with many uncertainties. For example, when the number of uncertainty N was set to 6, the first six parameters, $\boldsymbol{\rho} = (\mu_P, s_f, F, K_H, \mu_x, Y_{X/S})$, were considered, generating a six-dimensional random space. In this case study, each uncertainty was mathematically defined as: $\rho_i = \langle \rho_i \rangle (1 + \sigma r_i)$, where $\langle \rho_i \rangle$ is the mean value of the model parameter, which can be found in Mandur and Budman (2014), and σ was set to 0.05. Further, r_i is a random variable which is uniformly distributed in the range of $[-1, 1]$. The product of σr_i was used in this work to define uncertainty in each parameter. Note that, all random variables were

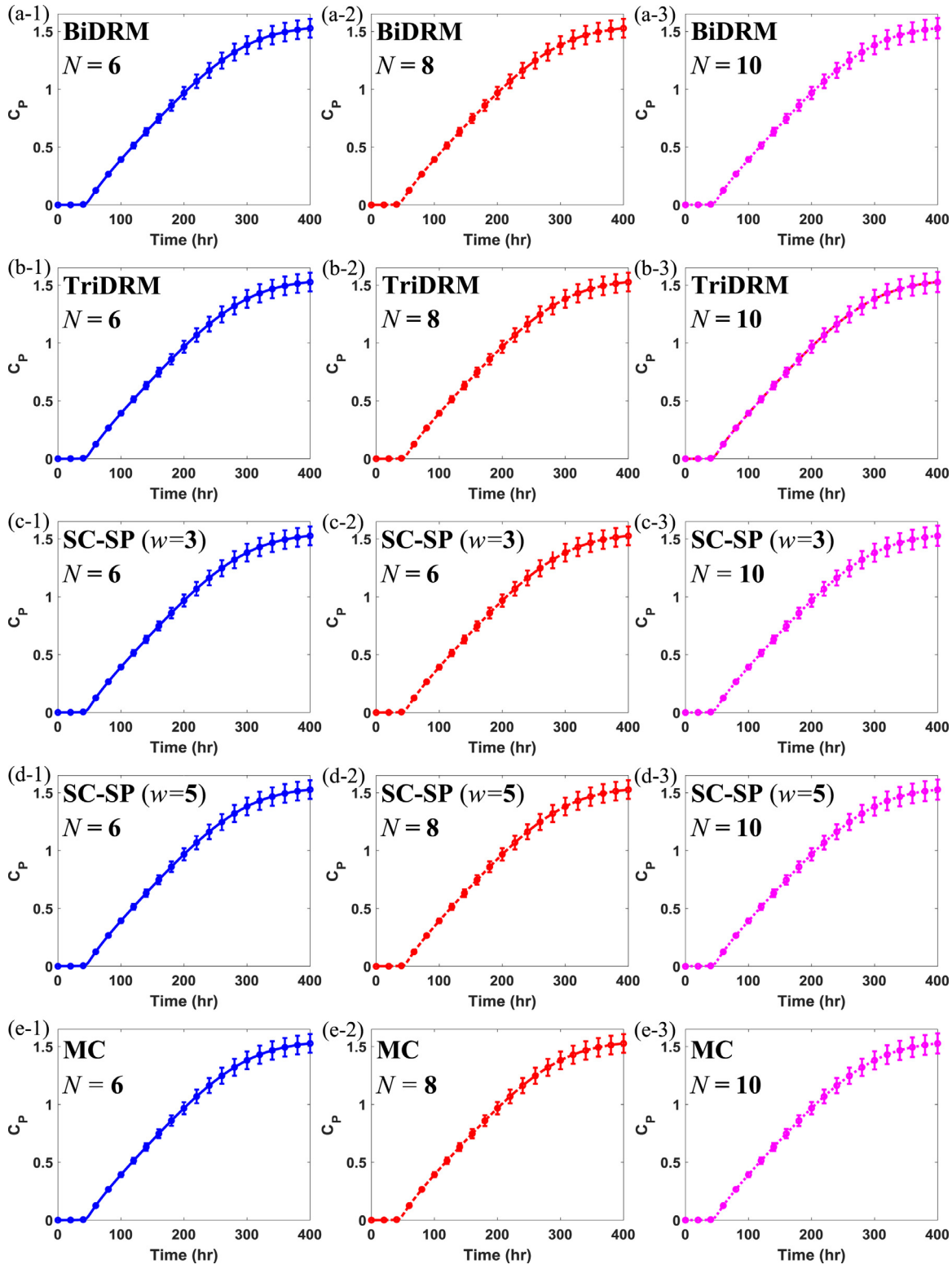

Fig. 4. UQ results of C_P with different methods and number of uncertainties (N = 6, 8 and 10): (a-1) to (a-3) results of BiDRM-based SG projection; (b-1) to (b-3) results of TriDRM-based SG projection; (c-1) to (c-3) results of SC-SP with w = 3; (d-1) to (d-3) results of SC-SP with w = 5; (e-1) to (e-3) results of MC. For the SC-SP, the Clenshaw-Curtis quadrature rules were used to generate sparse grid points. When w was set to 3, the number of sparse grid points was 389, 849, and 1581 for N = 6, 8, and 10, respectively. When w was 5, 4865, 15,713, and 41,265 sparse grids were required for N = 6, 8, and 10, respectively. Moreover, MC simulations with 10^5 samples were used to validate the UQ accuracy. Note that the number of samples used in MC was selected based on sensitivity analysis by varying the total number of samples used in the simulations and by checking the relative error with respect to the deterministic model. We found, when 10^5 samples were used, as compared to larger numbers of samples ($>10^5$), the change in relative error was negligible. Thus, 10^5 samples were used to reduce computational cost in this case study.

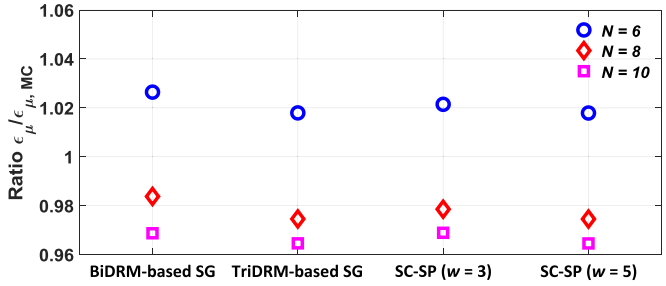

Fig. 5. Normalized relative errors of the mean values of C_P for different UQ methods, where N is the total number of uncertainties.

assumed to be independent and identically distributed in this case study.

4.2.1. Results of case 2—Fed-batch penicillin manufacturing process

Based on the UQ results in the first case study, BiDRM- and TriDRM-based gPC were compared to nonintrusive SC-SP method with two different approximation levels, $w = 3$ and $w = 5$, respectively. We excluded the HOUT-based SC since it was found to be less accurate in the benchmark case. And the full tensor grid points-based method (SC-FT) was not used for comparison, since we found that its accuracy is highly dependent on the number of grid points. When the number of uncertainties is increased and larger numbers of grid point are used, SC-FT increases the computational burden greatly.

The simulation results with different UQ methods are shown in Fig. 4, where each row of graphs presents the results of a specific UQ method, and each column presents the results with respect to different numbers of uncertainties (e.g., $N = 6$, 8, and 10). In addition, the solid line in each graph shows the mean value of the model response, the penicillin concentration C_P, while the error bars represent the uncertainty in C_P at a specific time point of simulations. The results of MC simulations are shown in the last row of Fig. 4 for comparison purposes. As seen, the intrusive UQ methods provide accurate UQ results as compared to other sampling-based nonintrusive UQ techniques. To quantify the accuracy of the proposed methods, the relative errors of mean response ϵ_μ defined in (40) were calculated for each method, and Fig. 5 shows the simulation results of the relative errors of C_P.

In Fig. 5, the relative error of C_P was calculated by averaging relative errors calculated at 20 time points over 400 h of simulations in Fig. 4. The relative error was also normalized with respect to the relative error calculated with MC for comparison purposes. As seen in Fig. 5, the normalized relative errors of C_P calculated with different UQ methods have similar results for a given N, the number of uncertainties. Compared to MC, intrusive and nonintrusive gPC-based methods provide accurate UQ results, since the normalized relative error is close to 1 as seen in Fig. 5. Specifically, we found that the relative error calculated with the TriDRM-based SG is almost identical to the result obtained with the SC-SP method, when the approximation level w was set to 5. And the relative error calculated with the BiDRM is similar to the result of SC-SP when w was set to 3. This shows that the proposed intrusive gDRM-based UQ can successfully address UQ challenges involving non-polynomial functions in the presence of many uncertainties. The efficiency of the gDRM-based UQ method will be further discussed in Section 4.4 in terms of computational time.

4.3. Case 3: autocrine signalling of live cells

In this case study, mathematical models describing the mitogen-activated protein kinase cascade were used to predict the dynamic behaviours of enzymes at three different stages of the cascade (Shvartsman et al., 2002; Xiu, 2007). This model has three enzymes, e_{1p}, e_{2p}, and e_{3p}, which describe the dimensionless concentrations of the active forms of enzymes as follows:

$$\frac{de_{1p}}{dt} = \frac{I(t)}{1 + G_4 e_{3p}} \frac{V_{max,1}\left(1 - e_{1p}\right)}{K_{m,1} + \left(1 - e_{1p}\right)} - \frac{V_{max,2} e_{1p}}{K_{m,2} + e_{1p}} \tag{45}$$

$$\frac{de_{2p}}{dt} = \frac{V_{max,3} e_{1p}\left(1 - e_{2p}\right)}{K_{m,3} + \left(1 - e_{2p}\right)} - \frac{V_{max,4} e_{2p}}{K_{m,4} + e_{2p}} \tag{46}$$

$$\frac{de_{3p}}{dt} = \frac{V_{max,5} e_{2p}\left(1 - e_{3p}\right)}{K_{m,5} + \left(1 - e_{3p}\right)} - \frac{V_{max,6} e_{3p}}{K_{m,6} + e_{3p}} \tag{47}$$

where G_4 is the gain of negative feedback, and the input signal is defined as $I(t)$. Model parameters in (45) through (47) include the maximal reaction velocity $V_{max,\ 1-6}$ and equilibrium Michaelis constant $K_{m,1-6}$. Details about the biological description of this model, including the model parameter values, can be found in Shvartsman et al. (2002). Uncertainty in model response e_{3p} resulting from parametric uncertainty, is considered in this work.

Like the second case study, intrusive and nonintrusive UQ methods were investigated. Following the sensitivity analysis described in our previous work (Son et al., 2018), simulations were first performed to rank the effect of parametric uncertainty on the model response, e_{3p}. Parameters $V_{\max,1-6}$ and $K_{m,1-6}$ can be ranked in descending order as: $V_{max,\ 3} > V_{max,\ 4} > V_{max,\ 1} > V_{max,\ 2} > V_{max,\ 5} > V_{max,\ 6} > K_{m,\ 4} > K_{m,\ 1} > K_{m,\ 3} > K_{m,\ 2} > K_{m,\ 6} > K_{m,\ 5}$. Following this, we considered three levels of parametric uncertainty: $N = 6$, 8, and 10. For example, the first six parameters, $V_{max,\ 3}$, $V_{max,\ 4}$, $V_{max,\ 1}$, $V_{max,\ 2}$, $V_{max,\ 5}$, and $V_{max,\ 6}$, were considered when N was set to 6. Further, uncertain parameters were mathematically defined as: $\rho_i = \langle \rho_i \rangle (1 + \sigma r_i)$, where ρ_i is the i^{th} uncertain parameter in $\boldsymbol{\rho}$, and $\langle \rho_i \rangle$ is the mean of each individual parametric uncertainty, which can be found in Shvartsman et al. (2002). In this case, σ was increased and set to 0.1 (in contrast to 0.05 in the previous case study) to verify UQ accuracy with respect to different levels of uncertainty. Additionally, a random variable r_i was used to introduce uncertainty, which is a constant number randomly selected in the range of $[-1, 1]$.

4.3.1. Results for case 3—Autocrine signalling of live cells

As in the second case study, BiDRM- and TriDRM-based SG, and SC-SP with different approximation levels were used to approximate uncertainty in the model response e_{3p}, which results from perturbations in parametric uncertainty. The results are shown in Fig. 6, where each row of graphs shows the results of a particular UQ method, and each column presents the results for a specific number of uncertainties. Legendre polynomials were chosen as the gPC basis functions for random variables, since we assumed that uncertainty was uniformly distributed. As seen in Fig. 6, the first two rows show simulation results calculated with the BiDRM and TriDRM methods, respectively. The third and fourth rows show the UQ results of the nonintrusive SC-SP method with different approximation levels. The solid line in each subplot shows the mean value of e_{3p}, while the error bars in each subplot show the variances estimated from the gPC at a particular time point. In addition, the last row in Fig. 6 shows the results of MC simulations. As seen in Fig. 6, we found that all methods provide accurate results as compared to MC.

As was done in case 2, the normalized relative error ϵ_μ of e_{3p} was calculated to compare UQ accuracy. Specifically, the average of relative errors at 20 simulation time points was first calculated and further normalized with respect to the average relative error of MC. Fig. 7 shows the normalized relative error for intrusive and nonintrusive methods. As seen, all methods provide almost identical relative errors for each specific number of uncertainties.

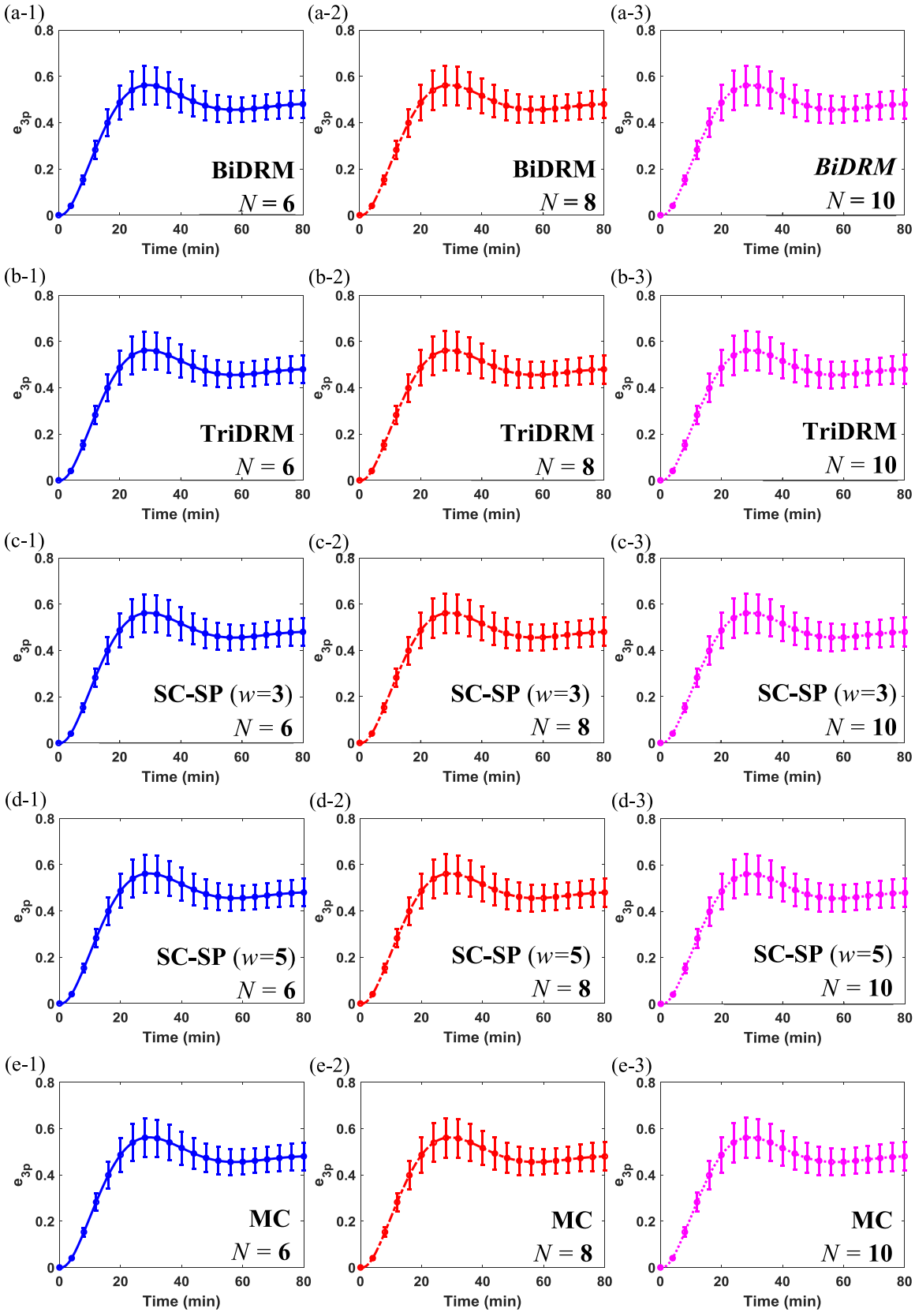

Fig. 6. UQ results of e_{3p} with different methods in $N = 6$, 8 and 10: (a-1) to (a-3) results of BiDRM-based SG; (b-1) to (b-3) results of TriDRM-based SG in $N = 6$, 8 and 10 respectively; (c-1) to (c-3) results of SC-SP with $w = 3$; (d-1) to (d-3) results of SC-SP with $w = 5$; (e-1) to (e-3) results of MC in $N = 6$, 8 and 10 respectively. For SC-SP method, the approximation level was set to 3 in the third row, which means that 389, 849, and 1581 sparse grid points were used, when N is set to 6, 8, and 10, respectively. Whereas, the fourth row shows the results of SC-SP, when the approximation level was set to 5. Thus, 4865, 15,713, and 41,265 sparse grid points were used for $N = 6$, 8, and 10, respectively. For MC, 10^5 samples were used for each of the input parametric uncertainty.

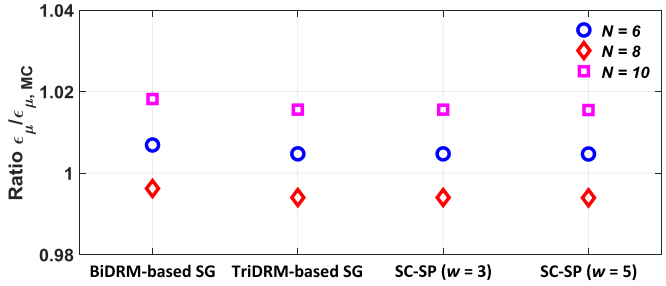

Fig. 7. Normalized relative errors of the mean values of e_{3p} for different UQ methods, where N is the total number of uncertainties.

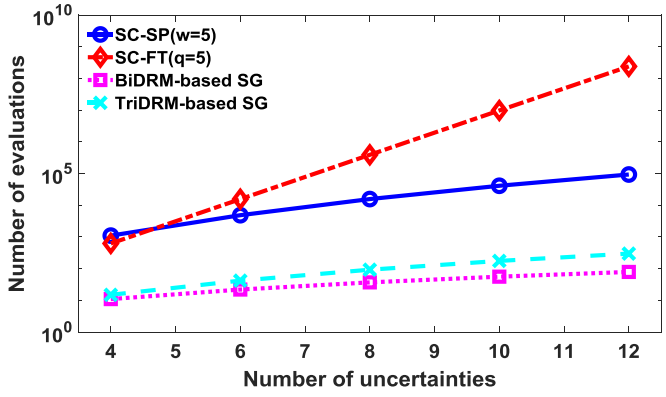

Fig. 8. Number of function evaluations with different UQ approaches. For the nonintrusive stochastic collocation (SC) method with a full tensor product grid, 5 collocation points were used for each uncertainty. In contrast, for the SC-based Smolyak method (SP), the approximation level was set to 5.

This further shows the potential of the proposed gDRM-based SG method to deal with complex problems.

4.4. Computational efficiency

The efficiency of different UQ methods can be also evaluated in terms of computational time. For each method, computational time was estimated from the required simulation runs. For example, the time required to calculate lower-dimensional integrals was measured for the gDRM, since these integrals are used to approximate high dimensional ones in SG projection and their calculation accounts for most of the computational effort. As seen in (22), N one-dimensional and $\binom{N}{2}$ two-dimensional integrals must be computed for the BiDRM. Similarly, the TriDRM requires calculating N one-dimensional, $\binom{N}{2}$ two-dimensional, and $\binom{N}{3}$ three-dimensional integrals. In contrast, for the nonintrusive UQ methods such as the SC-SP, computational time is closely related to the total number of collocation (or sparse grid) points. Thus, the computational time was quantified in terms of the number of collocation points required for calculating gPC coefficients in (24). For clarity, Fig. 8 shows the total number of simulation-runs for each method under different numbers of uncertainties. To generate sparse grid points for SC-SP in Fig. 8, Clenshaw-Curtis quadrature rules were used.

As seen in Fig. 8, the number of simulation runs required for each method is distinct, especially when the number of uncertainties is greater than 8. For example, the total number of simulation runs increases significantly for nonintrusive methods, as compared to intrusive methods. To better quantify computational time, case 2 was chosen. For the intrusive gDRM method, on average 0.04785, 0.02097, 0.01818, and 0.01123 s were required to calculate the three-, two-, one-dimensional integrals, and the constant term ($S = r$) in (22), respectively. When the number of uncertainties was set to 10, 1.137 and 6.879 s were required to calculate a gPC coefficient with the BiDRM and TriDRM methods, respectively. In contrast, when the SC-SP was used and the approximation level was set to 5, 41,265 grid points were required to calculate a gPC coefficient. Thus, 1.609 s were required to calculate gPC coefficients, since the time required for each grid point was about 3.9E-05 s. Compared to the SC-SP, the computational time required by BiDRM is about 29 percent points less than SC-SP. However, it can be argued that the computational time of TriDRM is larger than the nonintrusive SC-SP method.

To further assess the computational efficiency of the DRM-based UQ method, we estimated computational time by assuming the number of uncertainties can be as large as 40, since this will significantly increase the total number of required grid points for UQ with SC-SP. In this case, approximately 17 s and 8 min would be required to calculate a gPC coefficient using the BiDRM and TriDRM, respectively. In contrast, the SC-SP would need 29,458,657 grid points, which would take about 19 min, when the approximation level is set to 5. The obvious difference in computational cost between the intrusive gDRM and nonintrusive SC-SP is that for the latter, the number of required sparse grid points increases exponentially as the number of uncertainties increases. The significant reduction in computational cost for gDRM-based gPC is primarily the result of the smaller number of simulations required. For example, as seen in Fig. 8, the total number of gDRM simulations increases gradually as the number of uncertainties increases. Compared to SC-SP, this clearly shows the potential of gDRM to deal with many uncertainties. Note that the computational time was tested on a Core(TM) i5-8400 CPU 2.80 GHz office desktop with 12.0 GB of RAM. Additionally, recall that the difference in the normalized relative errors between the BiDRM and TriDRM is insignificant, 1.026 vs. 1.018, when N is 6 (Fig. 5). This shows the overall performance of the intrusive gDRM-based gPC in terms of UQ accuracy and computational time is superior to nonintrusive SC-SP and demonstrates its capability to deal with more complicated problems.

5. Conclusion

We present an intrusive uncertainty quantification (UQ) algorithm that provides an accurate quantification of how parametric uncertainty affects model predictions in nonlinear and complex systems. To alleviate the difficulty in calculating high-dimensional integrals involved in the stochastic Galerkin (SG) projection, the generalized dimension reduction method (gDRM) was combined with the generalized polynomial chaos (gPC) expansion. This converts a high-dimensional integral involved in the SG projection into several lower-dimensional ones that can be quickly calculated. The performance of the gDRM-based gPC was compared to other UQ methods in terms of UQ accuracy and computational time, including nonintrusive stochastic collocation and Monte Carlo simulations. Our results show the gDRM-based gPC can provide accurate UQ results and is computationally efficient when dealing with larger numbers of uncertainties (up to 10), thus laying the foundation to pursue more complicated problems in future work.

Declaration of Competing Interest

The authors declare that they have no known competing financial interests or personal relationships that could have appeared to influence the work reported in this paper.

Acknowledgments

This work was partially supported by the National Science Foundation, Division of Civil, Mechanical and Manufacturing Innovation (CMMI) under award No. 1727487.

Supplementary materials

Supplementary material associated with this article can be found, in the online version, at doi:10.1016/j.compchemeng.2019.106685.

References

Bajpai, R.K., Reuß, M., 1980. A mechanistic model for penicillin production. J. Chem. Technol. Biotechnol. 30, 332–344.
Birol, G., Ündey, C., Çinar, A., 2002. A modular simulation package for fed-batch fermentation: penicillin production. Comput. Chem. Eng. 26, 1553–1565.
Bradford, E., Imsland, L., 2019. Output feedback stochastic nonlinear model predictive control for batch processes. Comput. Chem. Eng. 126, 434–450.
Cheng, L., Lu, Z., Zhang, L., 2016. New spearman correlation based sensitivity index and its unscented transformation solutions. J. Eng. Mech. 142, 04015076.
Debusschere, B.J., Najm, H.N., Matta, A., Knio, O.M., Ghanem, R.G., Le Maître, O.P., 2003. Protein labeling reactions in electrochemical microchannel flow: numerical simulation and uncertainty propagation. Phys. Fluids 15, 2238–2250.
Debusschere, B.J., Najm, H.N., Pébay, P.P., Knio, O.M., Ghanem, R.G., Maître, O.P.L., 2004. Numerical challenges in the use of polynomial chaos representations for stochastic processes. SIAM J. Sci. Comput. 26, 698–719.
Du, Y., Budman, H., Duever, T., 2017. Parameter estimation for an inverse nonlinear stochastic problem: reactivity ratio studies in copolymerization. Macromol. Theory Simul. 26, 1600095.
Duong, P.L.T., Ali, W., Kwok, E., Lee, M., 2016. Uncertainty quantification and global sensitivity analysis of complex chemical process using a generalized polynomial chaos approach. Comput. Chem. Eng. 90, 23–30.
Eldred, M., Burkardt, J., 2009. Comparison of non-intrusive polynomial chaos and stochastic collocation methods for uncertainty quantification. In: Proceedings of the Forty-Seventh AIAA Aerospace Sciences Meeting Including the New Horizons Forum and Aerospace Exposition, pp. 1–20 AIAA Paper 2009-0976.
Gel, A., Garg, R., Tong, C., Shahnam, M., Guenther, C., 2013. Applying uncertainty quantification to multiphase flow computational fluid dynamics. Powder Technol. 242, 27–39.
Hill, J.M., Moore, R., 2004. Applied Mathematics Entering the 21st Century: Invited Talks from the ICIAM 2003 Congress. Society for Industrial and Applied Mathematics.
Huang, B., Du, X., 2006. Uncertainty analysis by dimension reduction integration and saddlepoint approximations. J. Mech. Des. 128, 26–33.
Judd, K.L., Maliar, L., Maliar, S., Valero, R., 2014. Smolyak method for solving dynamic economic models: Lagrange interpolation, anisotropic grid and adaptive domain. J. Econ. Dyn. Control 44, 92–123.
Julier, S.J., Uhlmann, J.K., 1997. Consistent, debiased method for converting between polar and Cartesian coordinate system. In: Proceedings of the SPIE AeroSense: Acquisition, Tracking and Pointing XI. International Society for Optics and Photonics, pp. 110–121.
Ma, D.L., Braatz, R.D., 2003. Robust identification and control of batch processes. Comput. Chem. Eng. 27, 1175–1184.
Mandur, J., Budman, H., 2014. Robust optimization of chemical processes using Bayesian description of parametric uncertainty. J. Process Control 24, 422–430.
Myung, I.J., 2003. Tutorial on maximum likelihood estimation. J. Math. Psychol. 47, 90–100.
Najm, H.N., 2009. Uncertainty quantification and polynomial chaos techniques in computational fluid dynamics. Annu. Rev. Fluid Mech. 41, 35–52.
Nobile, F., Tempone, R., Webster, C.G., 2008. A sparse grid stochastic collocation method for partial differential equations with random input data. SIAM J. Numer. Anal. 46, 2309–2345.
Schenkendorf, R., Xie, X., Krewer, U., 2019. An efficient polynomial chaos expansion strategy for active fault identification of chemical processes. Comput. Chem. Eng. 122, 228–237.
Shen, D.E., Braatz, R.D., 2016. Polynomial chaos-based robust design of systems with probabilistic uncertainties. AIChE J. 62, 3310–3318.
Shvartsman, S.Y., Hagan, M.P., Yacoub, A., Dent, P., Wiley, H.S., Lauffenburger, D.A., 2002. Autocrine loops with positive feedback enable context-dependent cell signaling. Am. J. Physiol. Cell Physiol. 282, C545–C559.
Smolyak, S.A., 1963. Quadrature and interpolation formulas for tensor products of certain classes of functions. Soviet Math. Dokl. 4, 240–243.
Son, J., Du, Y., 2019. Probabilistic surrogate models for uncertainty analysis: dimension reduction based polynomial chaos expansion. Int. J. Numer. Methods Eng. 2019, 1–20. doi:10.1002/nme.6262, In press.
Son, J., Du, Y., Du, D., 2018. Propagation of parametric uncertainty in Aliev-Panfilov model of cardiac excitation. In: Proceedings of the Fortieth Annual International Conference of the IEEE Engineering in Medicine and Biology Society (EMBC). IEEE, pp. 5450–5453.
Spanos, P.D., Zeldin, B.A., 1998. Monte carlo treatment of random fields: a broad perspective. Appl. Mech. Rev. 51, 219–237.
Wang, L., Cheng, X., 2015. Algorithm of gaussian sum filter based on high-order UKF for dynamic state estimation. Int. J. Control Autom. Syst. 13, 652–661.
Xiao, S., Lu, Z., 2018. Reliability analysis by combining higher-order unscented transformation and fourth-moment method. ASCE-ASME J. Risk Uncertain. Eng. Syst. A Civ. Eng. 4, 04017034.
Xiu, D., 2010. Numerical Methods for Stochastic Computations: A Spectral Method Approach. Princeton University Press, Princeton, NJ, USA.
Xiu, D., 2007. Efficient collocation approach for parametric uncertainty analysis. Commun. Comput. Phys. 2, 293–309.
Xiu, D., Hesthaven, J.S., 2005. High-order collocation methods for differential equations with random inputs. SIAM J. Sci. Comput. 27, 1118–1139.
Xiu, D., Karniadakis, G.E., 2002. The wiener–askey polynomial chaos for stochastic differential equations. SIAM J. Sci. Comput. 24, 619–644.
Xu, H., Rahman, S., 2004. A generalized dimension-reduction method for multidimensional integration in stochastic mechanics. Int. J. Numer. Methods Eng. 61, 1992–2019.
Xu, J., Dang, C., 2019. A new bivariate dimension reduction method for efficient structural reliability analysis. Mech. Syst. Signal Process. 115, 281–300.
Yeh, S.-T., 2002. Using trapezoidal rule for area under the curve calculation. In: Proceedings of the Twenty-Seventh Annual SAS User Group International Conference. SAS Institute Inc. 229–27.
Zhang, Y., Sahinidis, N.V., 2013. Uncertainty quantification in CO_2 sequestration using surrogate models from polynomial chaos expansion. Ind. Eng. Chem. Res. 52, 3121–3132.
Zhang, Y.-G., Huang, Y.-L., Wu, Z.-M., Li, N., 2014. A high order unscented Kalman filtering method. Acta Autom. Sin. 40, 838–848.